MEDWIN PUBLISHERS
Committed to create value for Researchers

Nanomedicine & Nanotechnology Open Access
ISSN: 2574-187X

Hydrogen Sensing with Villous Zinc Oxalate

Hsu C* and Li-ang Hsu

Department of chemical and materials engineering, Lunghwa University of Science and Technology, Taiwan

***Corresponding author**: Chen Hsu, Department of chemical and materials engineering, Lunghwa University of Science and Technology, 300, Sec. 1, Wanshou Rd. Guishan Shiang, Taoyuan country, Taiwan, E-mail: chenhsuemail@yahoo.com.tw

Research Article

Volume 3 Issue 1

Received Date: January 25, 2018

Published Date: February 1, 2018

DOI: 10.23880/nnoa-16000131

Abstract

Villous zinc oxalate (ZnC_2O_4) was synthesized using the sol–gel and laser method demonstrated in a previous paper, and the hydrogen-sensing properties of villous ZnC_2O_4 were investigated. The mixing ratio of reduced graphene oxide (RGO) to ZnO to form ZnC_2O_4 is predictive of its hydrogen-sensing capabilities. The microstructure evolution of villous structures was characterized by X-ray diffraction and field emission scanning electron microscopy techniques. Gas-sensing experiments tested response, recovery, and selectivity. The villous structure of ZnC_2O_4 can sense hydrogen at room temperature and an optimum operable temperature of 150°C at a specific C/Zn ratio. The strong hydrogen response is attributed to the villous structure and high C/Zn ratio of the 1:1 RGO to ZnO mixing ratio.

Keywords: Zinc Oxalate; Deduced Graphene Oxide; Zinc Oxide; Villous; Hydrogen Sensing

Introduction

Hydrogen sensing is an essential practice, especially in hydrogen-related industries, that can be is achieved using solid materials such as metal oxides and semiconductors [1-4]. An example of a common sensor is the resistivity-type metal-oxide hydrogen sensor [5]. Metal-oxide sensors act as hydrogen-adsorbing materials; the adsorbed hydrogen gas oxidizes to release electrons in combination with the adsorbent materials and the currents cause flow. The current signal can be used to detect the hydrogen concentration through electrochemical analysis. Adding certain selective metals such as platinum or gold can enhance sensitivity and selectivity [6]. These metals can operate at high temperatures, a wide band gap, and a high resistance value, all of which are conditions that typically hinder the application of metal-oxide-based gas sensors.

Nanomaterials such as graphene (GA), graphene oxide (GO), and reduced graphene oxide (RGO) have been developed to reduce photocatalytic degradation and improve hydrogen gas sensors [7,8]. However, graphene is not sensitive to hydrogen because of the small binding energy between H_2 molecules and the graphene surface [9-12]. GA is an ideal choice for loading into other materials such as metal oxide. To achieve greater sensitivity to H_2 molecules, a GA/ZnO nanocompositeis used to operate at the optimum operable temperature [12].

ZnO attraction of H atoms is explained as follows. The most common crystal structure of nanometer ZnO is hexagonal wurtzite [13-18]. When the $(00\bar{1})$ plane is taken as the surface, the crystal plane is composed of O atoms, leading to O atoms on the surface with excess charge δ^- [19,20]. O atoms have a strong ability to bind to

H (H^+) atoms. The O atom is located on the surface in an outwardly protruding position and with the H-atom-binding steric hindrance is conducive to the reaction. The plane can also attract and adsorb CO molecules on the $(00\bar{1})$ plane, and the interacting atoms on the plane are the H atom and C atom. The other sensing mechanism of metal oxide is based on the formation of a potential barrier due to the oxygen adsorbed on the metal-oxide surface for oxygen ionization and hydrogen modification of the potential barrier [7]. Although reducing hydrogen gas with sensing film is often a complex process, the reaction of ionized oxygen with hydrogen is usually represented by a simple irreversible reaction, expressed as follows:

$$O^-_{2ads} + 2H_2 \xrightarrow{k_r} 2H_2O + S + e^-_{free}$$

Where k_r is the rate coefficient of the reaction between reducing gas and adsorbed oxygen and S denotes an adsorption site.

The structure of ZnC_2O_4 has been studied [8] and can be thermally decomposed into ZnO, CO, and CO_2 [9]9 to prepare ZnO from ZnC_2O_4 [15,16]. In this study, hydrogen sensing used villous ZnC_2O_4 prepared through the sol–gel method. The optimized ZnC_2O_4 was used to control hydrolysis and condensation. This microstructure provided sites for hydrogen sensing.

Experimental Details

Methods for preparing and analyzing ZnC_2O_4 detailed in the authors' previous paper were employed [21-23]. The hydrogen-sensing configuration was sealed in a quartz tube. The hydrogen gas flowed at 10 sccm. The hydrogen response was measured using a precision LCR meter. The hydrogen-sensing properties of resistivity, recovery, and selectivity were measured.

Results and Discussion

(Figure 1) shows the X-ray diffraction spectra of ZnC_2O_4 with various RGO/ZnO ratios. Various symbols had the same meanings as those in a previous study and were interpreted as such [19]. The RGO/ZnO ratio increased with increasing amounts of β-ZnC_2O_4 in general. Except of that, the ratios β-ZnC_2O_4/α-ZnC_2O_4 are higher at the RGO/ZnO ratio of 1:1 than other RGO/ZnO ratios, calculated from the β-ZnC_2O_4 peak and α-ZnC_2O_4 peak highs in the curves.

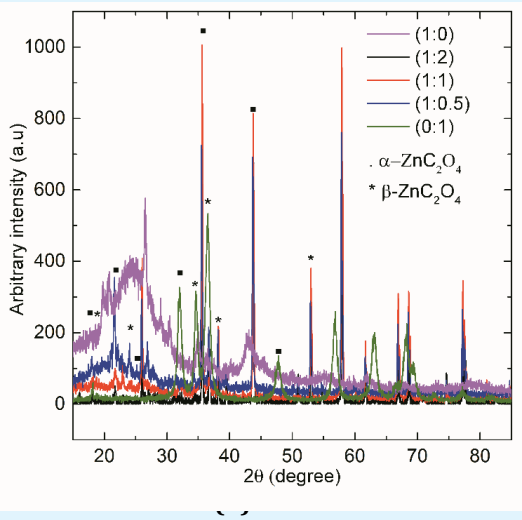

Figure 1: X-ray diffraction spectra of RGO, ZnO, and ZnC_2O_4 with various RGO/ZnO ratios obtained through the sol–gel method.

The previous statement is supported by the C/Zn ratio histogram versus composition, as shown in Figure 2. The 1:2 and 1:0.5 samples were under saturated with carbon (C/Zn) relative to the saturated 2:1 ratio of ZnC_2O_4. Conversely, the 1:1 ratio sample was oversaturated, denoting that the villous structure was not essential for sensing the hydrogen signal. Carbon oversaturation can be interpreted as enabling the sensing ability and provides a sensing site. The bonding sites of saturated ZnC_2O_4 are fully occupied with the atoms of Zn, C, and O. No additional bonding site is available for bonding with external hydrogen. Carbon oversaturation provides an interstitial position to bond the hydrogen. Because the villous structure has a high aspect ratio, a large area was provided for sensing sites.

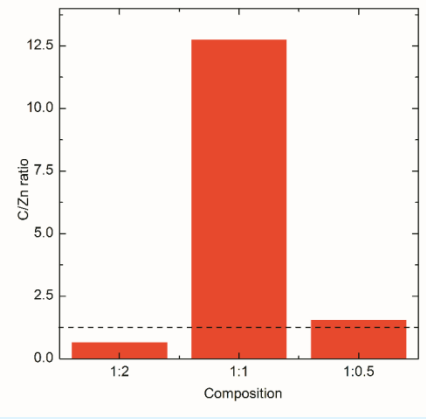

Figure 2: Histogram for various C/Zn ratios.

Scanning electron microscope images of RGO, ZnO, and ZnC_2O_4 after the micro-beam-laser process were shown in our previous paper [19]. Notably, the RGO/ZnO ratio of ZnC_2O_4 was 1:1. The chemical mapping is shown in Figure 3.

The C atoms of the RGO/ZnO 1:1 ratio are distributed around the internal and external phases and are higher than the O atoms of the other RGO/ZnO ratios. The villous sites increased by approximately three orders.

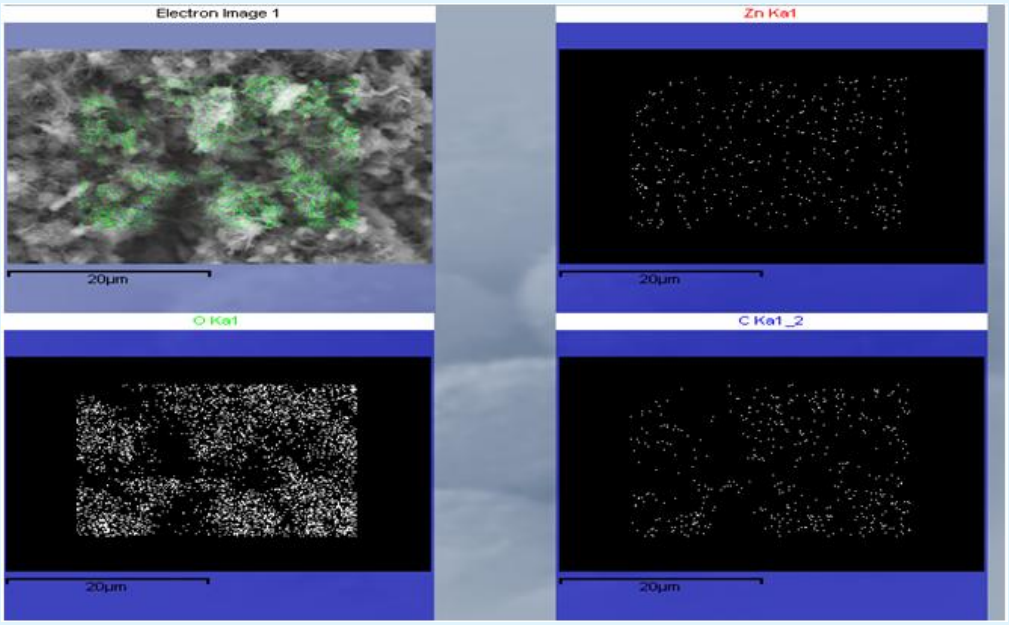

Figure 3: Field emission scanning electron microscopy maping images of samples with RGO/ZnO ratios of 1:1 after micro-beam-laser process.

Figure 4 represents the hydrogen responses of the RGO (1:0), ZnO (0:1), and ZnC_2O_4 prepared through the sol–gel method at RGO/ZnO ratios of 1:2, 1:1, and 1:0.5 at room temperature. The response from the RGO presented a low and flat signal; graphene is not sensitive to hydrogen because of the low binding energy between H_2 molecules and the graphene surface [10]. The response of ZnO had a high signal, denoting that ZnO is suitable for detecting hydrogen gas at room temperature. ZnO is a promising candidate for sensing applications. The ZnC_2O_4 signals varied with the RGO/ZnO ratios. The ratios of 1:2 and 1:0.5 had lower signals than does the RGO. Conversely, the 1:1 ratio has a higher signal than does the RGO. Furthermore, the 1:1 ratio signal was approximately one order lower than that of ZnO and increased over time in the initial stage.

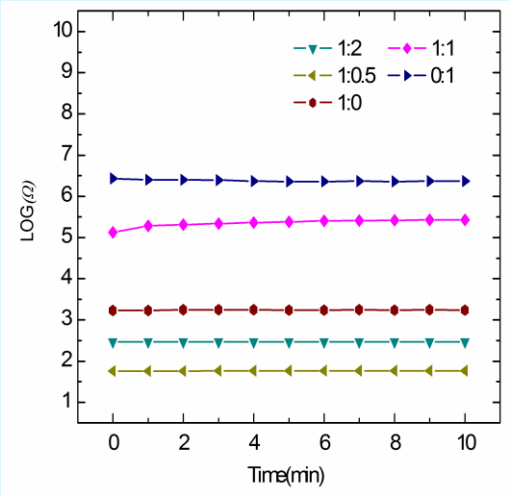

Figure 4: Hydrogen responses of RGO, ZnO, and ZnC_2O_4 at room temperature.

Figure 5 shows the hydrogen responses of the RGO, ZnO, and various ZnC_2O_4 ratios at 150°C. The 1:2 and 1:0.5 samples had lower response signals than did the RGO, and their response orders were identical to those at room temperature. The 1:1 sample exhibited a higher response than did the other ratios, and this response increased over time in the initial stage. The 1:1 sample exhibited the highest hydrogen response. The hydrogen sensing of ZnO exhibited a slightly weaker response than did the 1:1 sample at the optimum operable temperature of 150°C; this demonstrates that carbon oversaturation provides more bonding sites at the optimum operable temperature of 150°C.

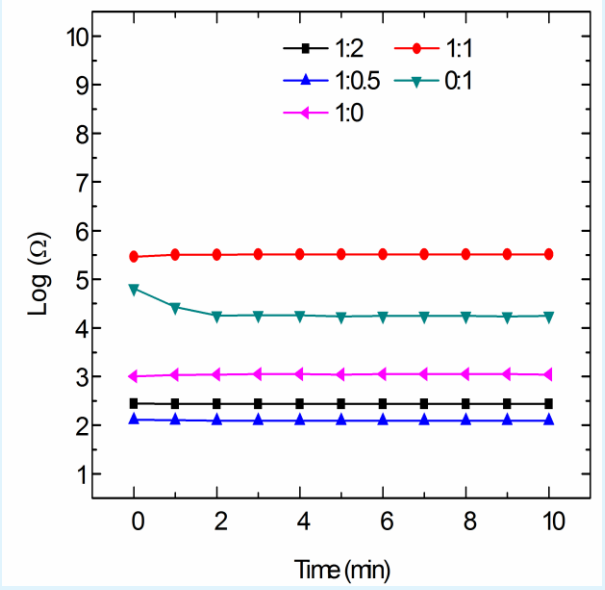

Figure 5: Hydrogen responses of RGO, ZnO, and various ZnC_2O_4 at 150°C.

Figure 6 illustrates the recovery experiments for the 1:1 sample at room temperature and at the optimum operable temperature of 150°C. The charging of hydrogen reached its peak after approximately 10 minutes and then released after approximately 3 more minutes at room temperature. At 150°C, hydrogen desorbed after approximately 1 minute. Furthermore, the signal reduced to only half of the saturated signal value at room temperature. The signal was fully recovered at the optimum operable temperature of 150°C.

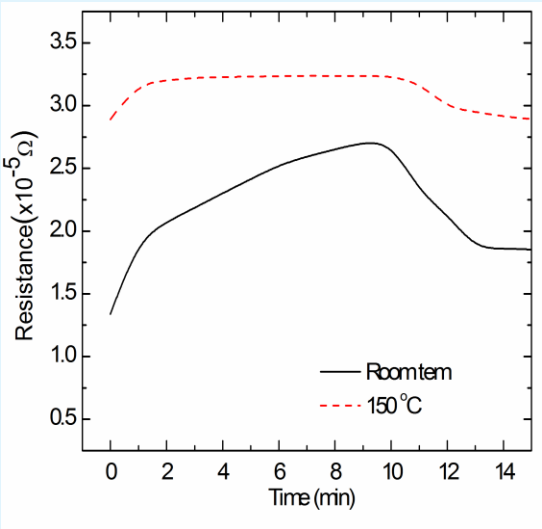

Figure 6: Recovery of the sample with a RGO/ZnO ratio of 1:1 at room temperature and 150°C.

The samples were exposed to oxygen gas and nitrogen gas to evaluate selectivity. Figure 7 shows the gas selectivity of ZnC_2O_4 when the gas flowed at 10 sccm at room temperature and 150°C. The oxygen and nitrogen gases exhibited low responses at both temperatures. The oxygen and nitrogen gases showed responses two times higher at 150°C than at room temperature. The oxygen and nitrogen responses were considerably lower than those from hydrogen sensing; this demonstrates that ZnC_2O_4 selectively responds to hydrogen gas but not to oxygen or nitrogen.

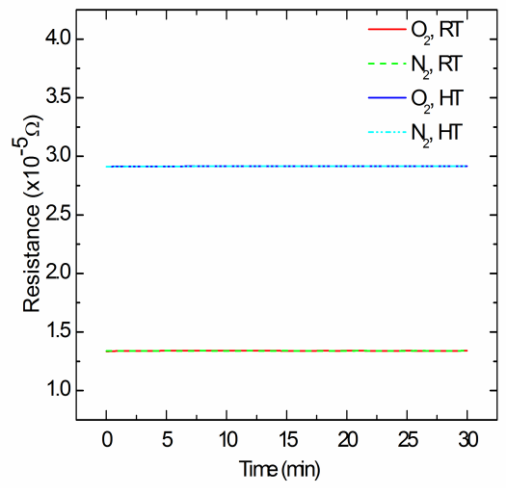

Figure 7: Gas selectivity of ZnC_2O_4 when flowed at 10 sccm at room temperature (RT) and a high temperature (HT) of 150°C.

The sensing mechanism of metal oxide is attributed to the formation of a potential barrier due to the oxygen adsorbed on the metal-oxide surface for ionization; hydrogen modifies this potential barrier [7]. In this study, the villous structure of ZnC_2O_4 produced high-density and high-aspect-ratio protrusions.

The sensing ability was displayed only on the carbon-oversaturated sample with a RGO/ZnO ratio of 1:1, which provided the adsorption site *S* for the sensing site. Therefore, this mechanism cannot fully explain the adsorption site. The adsorbed hydrogen and ionized oxygen reacted at the carbon-oversaturated site to produce electrons. The produced electrons were difficult to shift in ZnC_2O_4 and the resistivity increased. The results demonstrated the superior sensing ability of ZnC_2O_4 to ZnO, especially at the optimum operable temperature of 150°C.

The hydrogen sensing of ZnC_2O_4 cannot explain the mechanism of ZnO. Initially, α- and β-ZnC_2O_4 exhibited bonding similar to that of the $(00\bar{1})$ plane lead to O atoms with excess charge δ^- and surface activity. O atoms have a strong ability to bind to H (H^+) atoms on their surfaces; however the O atom cannot explain the specimen with the 1:1 RGO/ZnO ratio. When the oversaturation of RGO carbon joins with the O atom and changes the bonding angle to reveal the C atom on the surface in an outwardly protruding position, H atom binding is conducive to the reaction. The interacting atoms on the plane were H and C with a C/Zn ratio of approximately 1:1. Therefore, the hydrogen sensing of ZnC_2O_4 is attributed to the oversaturation of carbon binding with hydrogen instead of oxygen.

The villous structure of zinc oxalate (ZnC_2O_4) produces high-density and high-aspect-ratio protrusions. Furthermore, the carbon oversaturation in the 1:1 RGO/ZnO ratio sample provides the adsorption site *S* for sensing hydrogen. Consequently, the adsorbed hydrogen and ionized oxygen react at the carbon-oversaturated site. The results of this experiment demonstrate that the sensing ability of ZnC_2O_4 is superior to that of ZnO, especially at the optimum operable temperature.

Conclusions

In this study, the hydrogen-sensing properties of ZnC_2O_4 were attributed to the oversaturation of C atoms interacting with H rather than O atoms. When the RGO/ZnO ratio approached 1:1, the high C/Zn ratio provided adsorption sites for hydrogen sensing. These samples exhibited high hydrogen responses at room temperature and an optimum operable temperature of 150°C. Furthermore, the sensing selectivity of ZnC_2O_4 prefers to adsorb hydrogen rather than oxygen and nitrogen.

References

1. Katsuki A, Fukui K (1998) H_2 selective gas sensor based on SnO_2. Sensors and Actuators B Chemical 52(1-2): 30-37.

2. Ippolito SJ, Kandasamy S, Kalantar-zadeh WK, Wlodarski W (2005) Hydrogen sensing characteristics of WO_3 thin film conductometric sensors activated by Pt and Au catalysts. Sensors and Actuators B Chemical 108(1-2): 154-158.

3. Lupan O, Chai G, Chow L (2008) Novel hydrogen gas sensor based on single ZnO nanorod. Microelectronic Engineering 85(11): 2220-2225.

4. Gaman LI (2008) Basic physics of semiconductor hydrogen sensors. Russian Physics Journal 51(4): 425-441.

5. Phan DT, Chung GS (2014) Characteristics of resistivity-type hydrogen sensing based on palladium-graphene nanocomposites. International Journal of hydrogen energy 39(1): 620-629.

6. Fields LL, Zheng JP, Cheng Y (2006) Room temperature low power hydrogen sensor based on a single tin oxide nanobelt. Apply Physics Letters 88: 263102.

7. Anand K, Singh O, Singh MP, Kaur J, Singh RC (2014) Hydrogen sensor based on graphene/ZnOnanocomposite. Sensors and Actuators B Chemical 195: 409-415.

8. Ameen S, Akhtar MS, Seo HK, Hyung SS (2013) Advanced ZnO-graphene oxide nanohybid and its photocatalytic applications. Materials Letters 100(1): 261-265.

9. Chen YL, Zhang CE, Deng C, Fei P, Zhong M, et al. (2013) Preparation of ZnO/GO composite material with highly photocatalytic performance via an improved two-step method. Chines Chemical Letters 24(6): 518-520.

10. Wu W, Liu H, Jauregui LA, Yu QK, Pillai R, et al. (2010) Water-scale synthesis of graphene by chemical vapor deposition and its application in hydrogen sensing. Sensors and Actuators B Chemical 150(1): 295-300.

11. Fan HG, Zhao XT, Yang JH, Shan XN, Yang LL, et al. (2012) ZnO-graphene composite for photocatalytic degradation of methylene blue dye. Catalysis Communications 29(5): 29-34.

12. Dresselhaus MS, Dresselhaus G, Hofmann M (2008) Raman spectroscopy as a probe of graphene and carbon nanotubes. Royal Society 28(366): 231-236.

13. Dong SI, Li YK, Sun JY, Yu CF, Li YH, et al. (2014) Facile synthesis of novel ZnO/RGO hybrid nanocomposites with enhanced catalytic performance for visible-light-driven. Materials Chemistry and Physics 145(3): 357-365.

14. Shang C, Barnabe A (2013) Structural study and phase transition investigation in a simple synthesis of porous architected-ZnO nanopowder. Materials Characterization 86: 206-211.

15. Małecka B, Drożdż-CieślEwa A, Małecki A (2004) Mechanism and kinetics of thermal decomposition of zinc oxide. Thermochemica Acta 423: 13-18.

16. Cui JS, Sun JB, Lin X, Li JW, Ma XZ, et al. (2014) Fabrication of hierarchical flower-like porous ZnO nanostructures from layer $ZnC_2O_4 \cdot 3Zn(OH)_2$ and gas sensing properties. Applied surface Science 308(30): 17-23.

17. Justin RC, Joshi RK, Varma KBR (2011) Synthesis from zinc oxalate, growth mechanism and optical properties of ZnO nano/micro structures. Cryst Res Technol 46(11): 1181-1188.

18. Xu P, Tang Q, Zhou Z (2013) Structural and electronic properties of graphene–ZnO interfaces dispersion-corrected density functional theory investigations. Nanotechnology 24(30): 305401.

19. Wang JX, Sun XW, Yang Y, Huang H, Lee YC, et al. (2006) Hydrothermally grown oriented ZnO nanorod arrays for gas sensing applications. Nanotechnology 17(19): 037.

20. Vayssieres H, Keis K, Lindquist SE, Hagfeldt A (2001) Purpose-Built Anisotropic Metal Oxide Material: 3D Highly Oriented Microrod Array of ZnO. J Phys Chem B 105(17): 3350-3352.

21. Hsu C, Hsu LA (2017) Fabrication and Characteristics of Villus Zinc Oxalate by using a Sol-Gel and Microbeam-Laser Method. Nanomed Nanotechnol 2(1): 000112.

22. Hsu C (2017) Features of phase-refined materials. Nanomed Nanotechnol 2(1): 000114.

23. Hsu C (2017) Relationships among Graphene, Zinc Oxide and Zinc Oxalate in Nanomedicine. Nanomed Nanotechnol 2(S1): 000S1-002.